

# Emergent elasticity and topological stability of solitons

Yangfan Hu\*

*Research Institute of Interdisciplinary Science, School of Materials Science and Engineering,  
Dongguan University of Technology, Dongguan, 523808, China.*

## Abstract

Since the 1950s, topological solitons have been used to describe elementary particles[1-3] and particle-like field configurations that appear in systems ranging from subatomic to cosmological scales[3-6]. Particles are topologically protected, for which transitions to states with different topological charges are restricted. However, formation and annihilation of solitons are universal in almost all branches of physics[7-16], which implies that topological protection collapses at certain condition unrevealed[17, 18]. Here, we show that solitons can be regarded as emergent elastic objects with spatially dependent stiffness, and a second-order topological phase transition initiates at its “softened” points, i.e., points with a vanishing eigenvalue of the “emergent stiffness matrix”[19]. For example, the kink-antikink solution of the sine-Gordon model[3, 4, 20] and the single-particle Kosterlitz-Thouless phase transition of an isolated magnetic skyrmion[21, 22] with fixed modulus are both second-order topological phase transitions, with softened points at the center and at the exterior boundary, respectively. Annihilation of an isolated skyrmion with changeable modulus at high magnetic field is a first-order topological phase transition initiated at the center with a sharply decreased yet not softened emergent stiffness. We anticipate our model to be a starting point for a general study of topological stability of solitons in all field theories.

## Main

Solitons are a special type of spatially dependent field solution. According to the general theory of emergent elasticity and topological stability[19], we propose the following topological stability criterion for solitons:

*The local stability of a static soliton solution is guaranteed by the positiveness of a matrix  $\mathbf{C}^Q$  at every space point the soliton occupies, where the components of  $\mathbf{C}^Q$  are functions of space. Local destabilization of a soliton (for a topological soliton, variation of the topological charge) is initiated*

\* Corresponding author: huyf@dgut.edu.cn

*when at least one of the eigenvalues of  $\mathbf{C}^Q$  approaches zero at a point (or points) of the soliton, and the related eigenvector determines the destruction mode. When the free energy density or potential energy density is related to gradients of the state variables,  $\mathbf{C}^Q$  is the domain emergent elastic stiffness matrix, whereas when the free energy density or potential energy density is unrelated to gradients of the state variables,  $\mathbf{C}^Q$  is the domain emergent displacement stiffness matrix.*

The extension of this topological stability criterion to dynamical soliton solutions requires further investigation, although we will provide a dynamical case in this work where it is applicable. Nevertheless, the “softened” points of a soliton where at least one of the eigenvalues of  $\mathbf{C}^Q$  approaches zero is important concerning the pattern evolution of the soliton over time. In the language of emergent elasticity, a soliton is considered an infinite number of “unit elementary volumes” connected by springs with spatially dependent stiffness, and the presence of “softened” points leads to localized modes, whose wave pattern is localized around the “softened” points, as illustrated in the lattice dynamics of crystals with a defect[23, 24]. This means that soliton pattern evolution will most significantly occur around the “softened” points when these localized modes are excited.

To show how this criterion works, we study the emergent elasticity of some 1D soliton solutions of the sine-Gordon model and isolated skyrmion solutions of the magnetization field in helimagnets and further analyze the topological stability of these solutions under various thermodynamic parameters. The general procedure is as follows: (a) find the expression of the free energy density or the potential energy density of the problem; (b) find the analytical or numerical soliton solution and its variation with the parameter of interest; (c) determine the analytical form of the matrix  $\mathbf{C}^Q$  from the free energy density or the potential energy density, and by using the soliton solution given in step (b), obtain the distribution of  $\mathbf{C}^Q$  in space and its variation with the parameter of interest; and (d) calculate the eigenvalues of  $\mathbf{C}^Q$ , find the critical condition for topological stability at which one of the eigenvalues of  $\mathbf{C}^Q$  vanishes, and determine the critical parameter and the critical spatial point at which the eigenvalues of  $\mathbf{C}^Q$  vanish and the corresponding eigenvector, which shows the destruction mode.

### **Stability of the two-kink solutions of the sine-Gordon model**

Consider the two-kink solutions

$$y(x, t) = s_1 = 4 \tan^{-1} \left( \frac{\sinh x}{\cosh t} \right), \quad (3)$$

$$y(x, t) = s_2 = -4 \tan^{-1} \left( \frac{\sinh t}{\cosh x} \right) \quad (4)$$

of the 1D sine-Gordon model[3, 4, 20] with a Lagrangian density

$$L = \frac{1}{2} \dot{y}^2 - \frac{1}{2} y'^2 - (1 - \cos y), \quad (5)$$

where  $\dot{y} = \frac{\partial y}{\partial t}$ ,  $y' = \frac{\partial y}{\partial x}$  and the potential energy density  $\phi = \frac{1}{2} y'^2 + (1 - \cos y)$ .

In Eqs. (3, 4), all related parameters are set to unity for simplicity. Eq. (3) describes the elastic collision of two kinks with a repulsive interaction (Fig. 1(a)), while Eq. (4) describes the elastic collision of a kink-antikink pair with an attractive interaction (Fig. 2(a)). For these two 1D soliton solutions, only one effective emergent stiffness coefficient exists according to the general theory of emergent elasticity and topological stability[19]:

$$C^e = y'^2, \quad (6)$$

which represents both the domain and range emergent stiffness coefficients[19]. For the two solutions given in Eqs. (3, 4), we have

$$C^{e1} = C^e(s_1) = \frac{16 \cosh^2 x \operatorname{sech}^2 t}{(1 + \operatorname{sech}^2 t \sinh^2 x)^2}, \quad (7)$$

$$C^{e2} = C^e(s_2) = \frac{64 \sinh^2 x \sinh^2 t}{(\cosh 2t + \cosh 2x)^2}. \quad (8)$$

Fig. 1(b) and Fig. 2(b) show the distributions of  $C^{e1}$  and  $C^{e2}$  at different times. In the kink-kink collision described by Eq. (3), the emergent stiffness at the collision point  $C^{e1}(x = 0, t)$  gradually increases as the two kinks approach each other and finally reaches its maximum at  $t = 0$  when the two kinks collide (Fig. 1(b)). This phenomenon resembles the collision of two elastic balls, which squeeze and stabilize each other after contact and harden the contact area.

In the kink-antikink collision described by Eq. (4), the kink and antikink scatter elastically and annihilate at  $t = 0$  (Fig. 1(a)). Interestingly, according to Eq. (8),  $C^{e2}(x = 0, t) = 0$  for all  $t$  (Fig. 2(b)), forming a topological instability point for both the kink and antikink. Regarding  $t$  as a parameter, we can describe the kink-antikink collision process by a topological phase transition, which is initiated at the contact point as well as the topological instability point  $x = 0$ . To see this, we calculate the topological charge of the left half-space

$$N_{lh} = \frac{1}{2\pi} \int_{-\infty}^0 s_2' dx = \frac{1}{2\pi} s_2(x = 0) = \frac{2}{\pi} \tan^{-1}(\sinh t), \quad (9)$$

which, at  $t < 0$ , represents the topological charge of the antikink occupying the left half-space. As shown in Fig. 2(c), this topological charge is not conserved and continuously varies with time. At  $t = 0$ ,  $N_{lh}$  reaches zero and increases as  $t$  increases, which means that the kink and the antikink have moved pass each other at  $t = 0$ , and for  $t > 0$ , the kink occupies the left half-space.

### Stability of an isolated skyrmion in chiral magnets under an applied magnetic field

We then consider the three-dimensional magnetization vector field in B20 chiral magnets at low temperatures, which permits a static soliton solution called an isolated magnetic skyrmion of the Bloch type[21, 22] (Fig. 3(a)). The potential energy density of the system is given in a rescaled form[25] as

$$\phi = \sum_{i=1}^3 \left( \frac{\partial \mathbf{m}}{\partial x_i} \right)^2 - 2\mathbf{b} \cdot \mathbf{m} + \mathbf{m} \cdot (\nabla \times \mathbf{m}), \quad (10)$$

where the vector field  $\mathbf{m}$  denotes the magnetization, whose length is restricted to be 1 in this model.  $\mathbf{b}$  denotes the external magnetic field vector, and we assume here that  $\mathbf{b} = [0, 0, b]^T$ . The functional given in Eq. (10) can also be applied to describe skyrmions in liquid crystals[26]. We describe the problem in cylindrical coordinates  $\mathbf{x} = [\rho \cos\varphi, \rho \sin\varphi, z]^T$ , and the isolated skyrmion solution takes the form

$$\mathbf{m} = [-\sin\theta(\rho)\sin\varphi, \sin\theta(\rho)\cos\varphi, \cos\theta]^T, \quad (11)$$

where  $\theta(\rho)$  is to be numerically determined through minimization of  $\int \phi dV$  with the boundary conditions  $\theta(0) = \pi$  and  $\theta(R) = 0$ . In Fig. 3(c), the profile of  $\theta(\rho)$  solved at different values of  $b$  is shown. An isolated skyrmion is a two-dimensional symmetrical structure of magnetization with radius  $R$ , whose dependence on  $b$  is shown in Fig. 3(b). According to the theory of emergent elasticity and topological stability for 3D vector fields (see Methods for details), the emergent stiffness matrix for the isolated skyrmion solution given in Eq. (11) can be diagonalized in polar coordinates, and we have four diagonal elements:  $C_{\rho\rho}^e = 2\theta'^2(\rho)$ ,  $C_{\varphi\varphi}^e = \frac{2\sin^2\theta(\rho)}{\rho^2}$ ,  $C_{\gamma\gamma}^e = 2\left(\theta'^2(\rho) + \frac{\sin^2\theta(\rho)}{\rho^2}\right)$ , and  $C^{\omega_3} = \frac{2\sin^2\theta(\rho)}{\rho^2} + 2\theta'^2(\rho)$ . *The positive definiteness of these four coefficients at every spatial point occupied by an isolated skyrmion guarantees its topological stability. In contrast, when any one of these four parameters vanishes at any spatial point, the topological stability of an isolated skyrmion is broken, and the corresponding deformation modes are as follows:  $C_{\rho\rho}^e$  and  $C_{\varphi\varphi}^e$  correspond to emergent elongation in the  $\rho$  and  $\varphi$  directions,*

respectively, in the  $\rho - \varphi$  plane,  $C_{\gamma\gamma}^e$  corresponds to emergent shearing in the  $\rho - \varphi$  plane, and  $C^{\omega_3}$  corresponds to emergent rotation in the  $\rho - \varphi$  plane. The distribution of these four emergent stiffness coefficients as functions of  $\rho$  at different values of  $b$  are plotted in Fig. 3(d-g).

Due to the external boundary condition  $\theta(R) = 0$ , we always have  $C_{\varphi\varphi}^e(\rho = R) = 0$ , which means that an isolated skyrmion is intrinsically topologically unstable with respect to any disturbance that breaks the axial symmetry at  $\rho = R$ . In contrast, the topological stability of a skyrmion with respect to an axially symmetric disturbance (e.g., a change in a homogeneous magnetic field  $b$  along the  $z$  axis) is determined by  $C_{\rho\rho}^e$ . A well-known fact is that as  $b$  increases to some critical value  $b_c$ ,  $R$  approaches infinity[21] (Fig. 3(b)), characterizing a transition from a localized state to a state that occupies the whole space. As shown in Fig. 3(b), this transition is induced by softening of  $C_{\rho\rho}^e(\rho = R)$  at  $R \rightarrow \infty$ . This phenomenon can be regarded as the single particle version of the Kosterlitz-Thouless phase transition[4-5], so we call it a single-particle Kosterlitz-Thouless (SPKT) phase transition. It is a topological phase transition because the form of the solution does not change or become unstable, but we can find an appropriate order parameter: the averaged topological density  $\rho_t = \frac{1}{4\pi^2 R^2} \int \mathbf{m} \cdot (\mathbf{m}_x \times \mathbf{m}_y) dS$ . For finite  $R$ ,  $\rho_t$  is a finite real number, and for  $R \rightarrow \infty$ ,  $\rho_t \rightarrow 0$ . Nevertheless, this transition does not change the topological charge of the whole space because  $C_{\rho\rho}^e$  only approaches zero at  $R \rightarrow \infty$ , so for any spatial point that can be defined,  $C_{\rho\rho}^e$  is still positive.

Eq. (10) describes a magnetization field with fixed modulus, i.e., the length of  $\mathbf{m}$  defined in Eq. (11) is always 1. For such a model, we find that the SPKT phase transition is the only transition that exists by increasing  $b$ . This means that regardless of how strong the magnetic field we apply is, the isolated skyrmion will not annihilate. To study annihilation of an isolated skyrmion, we have to consider a magnetization field with changeable modulus, which is usually described by the following rescaled potential energy density:

$$\phi = \sum_{i=1}^3 \left( \frac{\partial \mathbf{m}}{\partial x_i} \right)^2 - 2\mathbf{b} \cdot \mathbf{m} + \mathbf{m} \cdot (\nabla \times \mathbf{m}) + \tilde{T} \mathbf{m}^2 + \mathbf{m}^4, \quad (12)$$

where  $\tilde{T}$  is the rescaled temperature. For such a model, Eq. (11) changes to

$$\mathbf{m} = m(\rho) [-\sin\theta(\rho)\sin\varphi, \sin\theta(\rho)\cos\varphi, \cos\theta]^T, \quad (13)$$

and similarly, we have four diagonal elements of the emergent stiffness matrix:  $C_{\rho\rho}^e = 2[m'^2(\rho) + m^2(\rho)\theta'^2(\rho)]$ ,  $C_{\varphi\varphi}^e = \frac{2m^2(\rho)\sin^2\theta(\rho)}{\rho^2}$ ,  $C_3^e = 4[m'^2(\rho) + m^2(\rho)\theta'^2(\rho)]$ , and  $C_4^e =$

$4m^2(\rho) \frac{\sin^2 \theta(\rho)}{\rho^2}$ , where the eigenvectors of  $C_3^e$  and  $C_4^e$  are shown in the Methods section. Here, the parameter of interest is the homogeneous magnetic field  $b$  applied along the  $z$  axis, which corresponds to axially symmetric loading, and the only effective emergent stiffness coefficient is  $C_{\rho\rho}^e$ . For the solution of the isolated skyrmion determined for this model, two first-order phase transitions occur as the magnetic field increases from zero: as shown in Fig. 4(f), the SPKT phase transition occurs at approximately  $b_s = 1.11$ , and the annihilation phase transition occurs at approximately  $b_a = 1.365$ , where the isolated skyrmion annihilates itself and the resulting state is the ferromagnetic phase. The phenomenon of the SPKT phase transition resembles that of the isolated skyrmion given by Eq. (11): around  $b_s$ ,  $\theta(\rho)$  changes smoothly near  $\rho = R$  (Fig. 4(a)), and  $C_{\rho\rho}^e(\rho = R)$  gradually approaches zero (red curve in Fig. 4(f)). However, further analysis shows that this is a first-order phase transition. In Fig. 4(d), we show the curves of free energy density  $\phi$  minimized at different values of radius  $R$  at different values of  $b$ . The circular blue dots mark the equilibrium values of  $R$  for different  $b$  ( $R$  increases with  $b$ ), and at  $b_s = 1.11$ , a local maximum point marked by a blue star appears in the  $\phi(R)$  curve. For  $R$  larger than the marked blue star,  $\phi(R)$  decreases with  $R$  until infinity; i.e., when  $b$  reaches 1.11, the equilibrium value of  $R$  jumps from approximately 4.8 to infinity, indicating a first-order phase transition.

The first-order character of the annihilation phase transition is more obvious. Near  $b_a$ , we see that  $C_{\rho\rho}^e$  decreases at  $\rho = 0$ , but not to zero (black curve in Fig. 4(f)). Since  $C_{\rho\rho}^e(\rho = 0) = 2m^2(\rho = 0)\theta'^2(\rho = 0)$ , we further calculate the distributions of  $m(\rho)$  (Fig. 4(b)) and  $\theta'(\rho)$  (Fig. 4(c)) at different  $b$  and find that near  $b_a$ ,  $m(\rho)$  drastically drops at  $\rho = 0$ , which is the dominant reason for the annihilation of the skyrmion. In contrast,  $|\theta'(\rho)|$  drastically increases around  $b_a$  at  $\rho = 0$ , which smooths the softening of  $C_{\rho\rho}^e(\rho = 0)$ . Nevertheless, the sudden drop in  $C_{\rho\rho}^e(\rho = 0)$  near  $b_a$  still provides a signal for the occurrence of the annihilation phase transition, showing that the analysis of emergent elasticity provides an effective sign for the first-order topological phase transition. The annihilation phase transition is a more severe phase transition than the SPKT phase transition in the following two senses: (a) the topological charge of the solution before and after the annihilation phase transition is 1 and 0, while the topological charge is conserved during the SPKT phase transition; (b) after the annihilation phase transition, the solution of the magnetization field

changes from nontrivial to trivial, while the solution maintains its form during the SPKT phase transition. We show in a subsequent work that by incorporating the effect of mechanical torsion, the annihilation phase transition of an isolated skyrmion in a nanodisk can be tuned from a first-order phase transition to a second-order phase transition[27].

## Outlook

The concept of topology provides a way to categorize solitons and further qualitatively explain particle stability by topological protection. However, the topological property of a soliton will change at some critical conditions, which is determined by the internal structure of a soliton, or more specifically, by the emergent stiffness at the “softened” points of a soliton. This cannot be revealed by calculating any global topological quantity, such as the topological charge. The stability criterion established is to be further applied to other classical soliton models and their quantum mechanical counterparts. In terms of the stability criterion itself, an important extension to be further developed is its dynamical version.

## Methods

Emergent elasticity and topological stability of a vector field in 3D space

For an arbitrary vector solution  $\mathbf{p}(\mathbf{x}) = \tilde{\mathbf{p}}(\mathbf{x})$  with *three* components in 3D space, a general form of *critical condition of topological stability can be derived following our previous work[hu] and is presented as follow. For  $\phi = \phi(\mathbf{x}, p_i, p_{j,k})$ , we do the following replacements concerning domain emergent elasticity:  $p_i(\mathbf{x}) \rightarrow \tilde{p}_i(\mathbf{x} - \mathbf{u}(\mathbf{x}))$ ,  $p_{j,k}(\mathbf{x}) \rightarrow \tilde{p}_{j,i}(\mathbf{x} - \mathbf{u}(\mathbf{x}))(\delta_{ik} - u_{i,k}) = \tilde{p}_{j,i}(\mathbf{x} - \mathbf{u}(\mathbf{x}))(\delta_{ik} - (\varepsilon_{ik} + \epsilon_{ikl}\omega_l))$ , and obtain  $\phi_u = \phi(\mathbf{x}, \tilde{p}_i(\mathbf{x} - \mathbf{u}(\mathbf{x})), \tilde{p}_{j,i}(\mathbf{x} - \mathbf{u}(\mathbf{x}))(\delta_{ik} - (\varepsilon_{ik} + \epsilon_{ikl}\omega_l)))$ , where  $\varepsilon_{ik} = \frac{1}{2}(u_{i,k} + u_{k,i})$  is the domain emergent elastic strains and  $\epsilon_{ikl}\omega_l = \frac{1}{2}(u_{i,k} - u_{k,i})$ , with  $\omega_l$  the emergent rotational angle and  $\epsilon_{ikl}$  are components of the Levi-Civita tensor according to relevant definition in solid mechanics. In 3D space, we can define the following domain emergent elastic deformation vector*

$$\boldsymbol{\varepsilon} = [\varepsilon_{11} \quad \varepsilon_{22} \quad \varepsilon_{33} \quad \varepsilon_{23} \quad \varepsilon_{13} \quad \varepsilon_{12} \quad \omega_1 \quad \omega_2 \quad \omega_3]^T, \quad (14)$$

and the domain emergent elastic stiffness matrix  $\mathbf{C}^{\varepsilon}$  is derived by

$$C_{ij}^{\varepsilon} = \left( \frac{\partial^2 \phi_u}{\partial \varepsilon_i \partial \varepsilon_j} \right)_{\mathbf{u}(\mathbf{x})=\mathbf{0}}. \quad (15)$$

The critical condition of topological stability in this case is **at some point or points in space, at least one of the eigenvalues of  $\mathbf{C}^{\varepsilon}$  drop to zero**. According to our previous study[hu], in this case the range emergent elastic stiffness matrix is equivalent to  $\mathbf{C}^{\varepsilon}$ , so that  $\mathbf{C}^{\varepsilon}$  can be referred to as the emergent elastic stiffness matrix.

For  $\phi = \phi(\mathbf{x}, p_i)$ , we do the following replacements concerning domain emergent elasticity:

$p_i(\mathbf{x}) \rightarrow \tilde{p}_i(\mathbf{x} - \mathbf{u}(\mathbf{x}))$ , and obtain  $\phi_u = \phi(\mathbf{x}, \tilde{p}_i(\mathbf{x} - \mathbf{u}(\mathbf{x})))$ , the state variable here is the emergent displacement vector

$$\mathbf{u} = [u_1 \quad u_2 \quad u_3]^T, \quad (16)$$

and the the domain emergent displacement stiffness matrix  $\mathbf{C}^u$  is derived by

$$C_{ij}^u = \left( \frac{\partial^2 \phi_u}{\partial u_i \partial u_j} \right)_{\mathbf{u}(\mathbf{x})=\mathbf{0}}. \quad (17)$$

The critical condition of topological stability in this case is **at some point or points in space, at least one of the eigenvalues of  $\mathbf{C}^{\varepsilon}$  drop to zero**. For range emergent elasticity of this case, a condition similar to that of the second order variation of  $\phi$  with respect to  $p_i$  can be obtained, so that  $\mathbf{C}^u$  can be referred to as the emergent displacement stiffness matrix.

Now we apply the general formula above to study the isolated magnetic skyrmion. The free energy density is given by eq. (10) (or eq. (12)), which corresponds to the case  $\phi = \phi(m_i, m_{j,k})$ , and the soliton solution is given by eq. (11) (or eq. (13)), which takes the form  $\mathbf{m} = \mathbf{m}(\rho) = \mathbf{m}(\sqrt{x^2 + y^2})$ . Since this is a 2D solution, eq. (14) reduces to

$$\boldsymbol{\varepsilon} = [\varepsilon_{11} \quad \varepsilon_{22} \quad \varepsilon_{12} \quad \omega_3]^T. \quad (18)$$

And for the free energy density given by eq. (10) (or eq. (12)), to obtain the expression of  $\phi_u$  we do the following replacements:  $m_{1,1} \rightarrow (1 - \varepsilon_{11})m_{1,1} - (\varepsilon_{12} - \omega_3)m_{1,2}$ ,  $m_{1,2} \rightarrow -(\varepsilon_{12} + \omega_3)m_{1,1} + (1 - \varepsilon_{22})m_{1,2}$ ,  $m_{2,1} \rightarrow (1 - \varepsilon_{11})m_{2,1} - (\varepsilon_{12} - \omega_3)m_{2,2}$ ,  $m_{2,2} \rightarrow -(\varepsilon_{12} + \omega_3)m_{2,1} + (1 - \varepsilon_{22})m_{2,2}$ ,  $m_{3,1} \rightarrow (1 - \varepsilon_{11})m_{3,1} - (\varepsilon_{12} - \omega_3)m_{3,2}$ ,  $m_{3,2} \rightarrow -(\varepsilon_{12} + \omega_3)m_{3,1} + (1 - \varepsilon_{22})m_{3,2}$ , and from eq. (15) the expressions of the emergent elastic stiffness matrix  $\mathbf{C}^{\varepsilon}$  can be derived in the Cartesian coordinates. Since the solution of isolated magnetic skyrmion in this case is axially symmetric, it is more convenient to study its emergent elastic stiffness in polar coordinates. To achieve this, we recall the following coordinate transformation relation:

$$\hat{\boldsymbol{\varepsilon}} = \mathbf{K}\boldsymbol{\varepsilon}, \quad (19)$$

where

$$\mathbf{K} = \begin{bmatrix} \cos^2 \varphi & \sin^2 \varphi & -\sin 2\varphi / 2 & 0 \\ \sin^2 \varphi & \cos^2 \varphi & \sin 2\varphi / 2 & 0 \\ \sin 2\varphi & -\sin 2\varphi & \cos 2\varphi & 0 \\ 0 & 0 & 0 & 1 \end{bmatrix}, \quad (20)$$

$$\hat{\boldsymbol{\varepsilon}} = [\varepsilon_{\rho\rho} \quad \varepsilon_{\varphi\varphi} \quad \varepsilon_{\rho\varphi} \quad \omega_3]^T. \quad (21)$$

The emergent elastic stiffness matrix presented in polar coordinates can be derived as

$$\hat{\mathbf{C}}^\varepsilon = \mathbf{K}^T \mathbf{C}^\varepsilon \mathbf{K}. \quad (22)$$

When  $\phi$  is given by eq. (10), we have after manipulation

$$\hat{\mathbf{C}}^\varepsilon = \begin{bmatrix} C_{\rho\rho}^e & 0 & 0 & 0 \\ 0 & C_{\varphi\varphi}^e & 0 & 0 \\ 0 & 0 & C_{\gamma\gamma}^e & 0 \\ 0 & 0 & 0 & C^{\omega_3} \end{bmatrix}, \quad (23)$$

where  $C_{\rho\rho}^e = 2\theta'^2(\rho)$ ,  $C_{\varphi\varphi}^e = \frac{2\sin^2\theta(\rho)}{\rho^2}$ ,  $C_{\gamma\gamma}^e = 2\left(\theta'^2(\rho) + \frac{\sin^2\theta(\rho)}{\rho^2}\right)$ , and  $C^{\omega_3} = \frac{2\sin^2\theta(\rho)}{\rho^2} + 2\theta'^2(\rho)$ . Since  $\hat{\mathbf{C}}^\varepsilon$  is already diagonal,  $C_{\rho\rho}^e$ ,  $C_{\varphi\varphi}^e$ ,  $C_{\gamma\gamma}^e$  and  $C^{\omega_3}$  are four eigenvalues of  $\hat{\mathbf{C}}^\varepsilon$  and the corresponding eigenvectors are  $[1 \ 0 \ 0 \ 0]^T$ ,  $[0 \ 1 \ 0 \ 0]^T$ ,  $[0 \ 0 \ 1 \ 0]^T$ , and  $[0 \ 0 \ 0 \ 1]^T$ , respectively.

When  $\phi$  is given by eq. (12), the four eigenvalues of  $\hat{\mathbf{C}}^\varepsilon$  are  $C_{\rho\rho}^e = 2[m'^2(\rho) + m^2(\rho)\theta'^2(\rho)]$ ,  $C_{\varphi\varphi}^e = \frac{2m^2(\rho)\sin^2\theta(\rho)}{\rho^2}$ ,  $C_3^e = 4[m'^2(\rho) + m^2(\rho)\theta'^2(\rho)]$ , and  $C_4^e = 4m^2(\rho)\frac{\sin^2\theta(\rho)}{\rho^2}$ , and the corresponding eigenvectors are  $[1 \ 0 \ 0 \ 0]^T$ ,  $[0 \ 1 \ 0 \ 0]^T$ ,  $[0 \ 0 \ 1 \ 1]^T$ , and  $[0 \ 0 \ -1 \ 1]^T$ , respectively.

### Acknowledgments

The work was supported by the NSFC (National Natural Science Foundation of China) through the funds with Grant Nos. 12172090, 11772360, 11832019, 11572355, the Natural Science Foundation of Guangdong Province (Grant No. 2019A1515012016), and Pearl River Nova Program of Guangzhou (Grant No. 201806010134).

### Author contributions

Y.H. conceived the idea and conducted the work.

### Competing interests

The authors declare no competing interests.

## References

- [1] Heisenberg, W. (1984). *Introduction to the unified field theory of elementary particles*. In *Scientific Review Papers, Talks, and Books Wissenschaftliche Übersichtsartikel, Vorträge und Bücher* (pp. 677-861). Springer, Berlin, Heidelberg.
- [2] Skyrme, T. H. (1961). *A non-linear field theory*. *Proc. R. Soc. Lond. Ser. A* 260, 127–138.
- [3] Weinberg, E. (2012). *Classical Solutions in Quantum Field Theory: Solitons and Instantons in High Energy Physics (Cambridge Monographs on Mathematical Physics)*. Cambridge: Cambridge University Press. doi:10.1017/CBO9781139017787
- [4] Manton, N., & Sutcliffe, P. (2004). *Topological Solitons (Cambridge Monographs on Mathematical Physics)*. Cambridge: Cambridge University Press. doi:10.1017/CBO9780511617034
- [5] Brown, G. E., & Rho, M. (2010). *The multifaceted skyrmion*. World Scientific.
- [6] Chaikin, P. M., Lubensky, T. C., & Witten, T. A. (1995). *Principles of condensed matter physics (Vol. 10)*. Cambridge: Cambridge university press.
- [7] Nguyen, J. H., Luo, D., & Hulet, R. G. (2017). *Formation of matter-wave soliton trains by modulational instability*. *Science*, 356(6336), 422-426.
- [8] Carr, L. D., & Brand, J. (2004). *Spontaneous soliton formation and modulational instability in Bose-Einstein condensates*. *Physical Review Letters*, 92(4), 040401.
- [9] Milde, P., Köhler, D., Seidel, J., Eng, L. M., Bauer, A., Chacon, A., ... & Rosch, A. (2013). *Unwinding of a skyrmion lattice by magnetic monopoles*. *Science*, 340(6136), 1076-1080.
- [10] Qi, X. L., Li, R., Zang, J., & Zhang, S. C. (2009). *Inducing a magnetic monopole with topological surface states*. *Science*, 323(5918), 1184-1187.
- [11] Scott, A. (1992). *Davydov's soliton*. *Physics Reports*, 217(1), 1-67.
- [12] Su, W., Schrieffer, J. R., & Heeger, A. J. (1979). *Solitons in polyacetylene*. *Physical Review Letters*, 42(25), 1698.
- [13] Khaykovich, L., Schreck, F., Ferrari, G., Bourdel, T., Cubizolles, J., Carr, L. D., ... & Salomon, C. (2002). *Formation of a matter-wave bright soliton*. *Science*, 296(5571), 1290-1293.

- [14] Fu, Q., Wang, P., Huang, C., Kartashov, Y. V., Torner, L., Konotop, V. V., & Ye, F. (2020). Optical soliton formation controlled by angle twisting in photonic moiré lattices. *Nature Photonics*, 14(11), 663-668.
- [15] Lee, T. D. (1987). Soliton stars and the critical masses of black holes. *Physical Review D*, 35(12), 3637.
- [16] Eto, M., Isozumi, Y., Nitta, M., Ohashi, K., & Sakai, N. (2005). Instantons in the Higgs phase. *Physical Review D*, 72(2), 025011.
- [17] Kuznetsov, E. A., Rubenchik, A. M., & Zakharov, V. E. (1986). Soliton stability in plasmas and hydrodynamics. *Physics Reports*, 142(3), 103-165.
- [18] Lee, T. D., & Pang, Y. (1992). Nontopological solitons. *Physics Reports*, 221(5-6), 251-350.
- [19] Hu, Y., (2022). General theory of emergent elasticity and topological stability. Submitted.
- [20] Perring, J. K., & Skyrme, T. H. R. (1962). A model unified field equation. *Nucl. Phys.*, 31, 550-555.
- [21] Roessler, U. K., Bogdanov, A. N., & Pfleiderer, C. (2006). Spontaneous skyrmion ground states in magnetic metals. *Nature*, 442(7104), 797-801.
- [22] Mühlbauer, S., Binz, B., Jonietz, F., Pfleiderer, C., Rosch, A., Neubauer, A., ... & Böni, P. (2009). Skyrmion lattice in a chiral magnet. *Science*, 323(5916), 915-919.
- [23] Born, M. & Huang, K. *Dynamical Theory of Crystal Lattices* (Clarendon, Oxford, 1954).
- [24] Mannheim, P. D. (1968). Influence of force-constant changes on the lattice dynamics of cubic crystals with point defects. *Physical Review*, 165(3), 1011.
- [25] Leonov, A. O., & Bogdanov, A. N. (2018). Crossover of skyrmion and helical modulations in noncentrosymmetric ferromagnets. *New Journal of Physics*, 20(4), 043017.
- [26] Leonov, A. O., Dragunov, I. E., Röbber, U. K., & Bogdanov, A. N. (2014). Theory of skyrmion states in liquid crystals. *Physical Review E*, 90(4), 042502.
- [27] Wan, X., Zhong, A., Hu, Y., Lan, X., and Wang, B. (2022). Helicity reversal and tricritical behavior of magnetization structures in helimagnet nanodisks under torsion. Submitted.

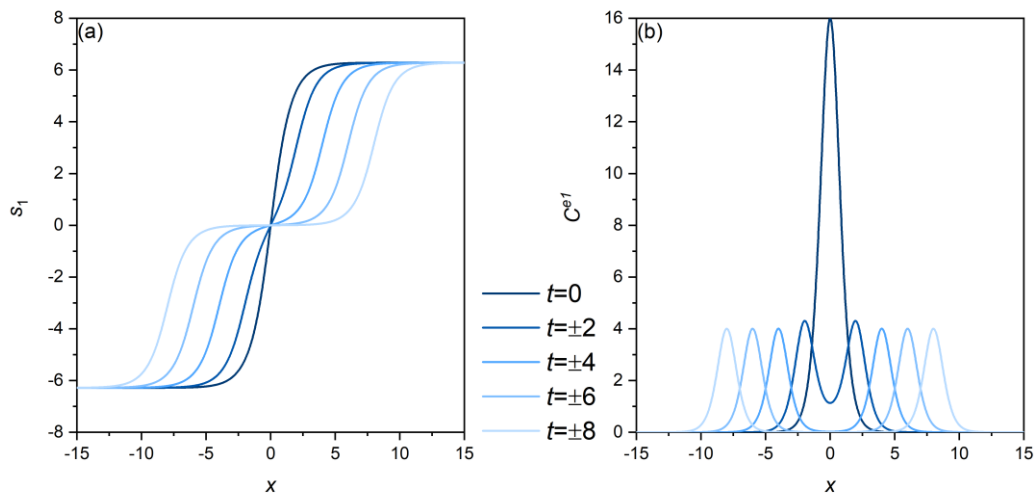


Figure 1. (a) Field pattern and (b) emergent stiffness  $C^{e1}$  of the kink-kink collision solution of the sine-Gordon model at different values of  $t$ .

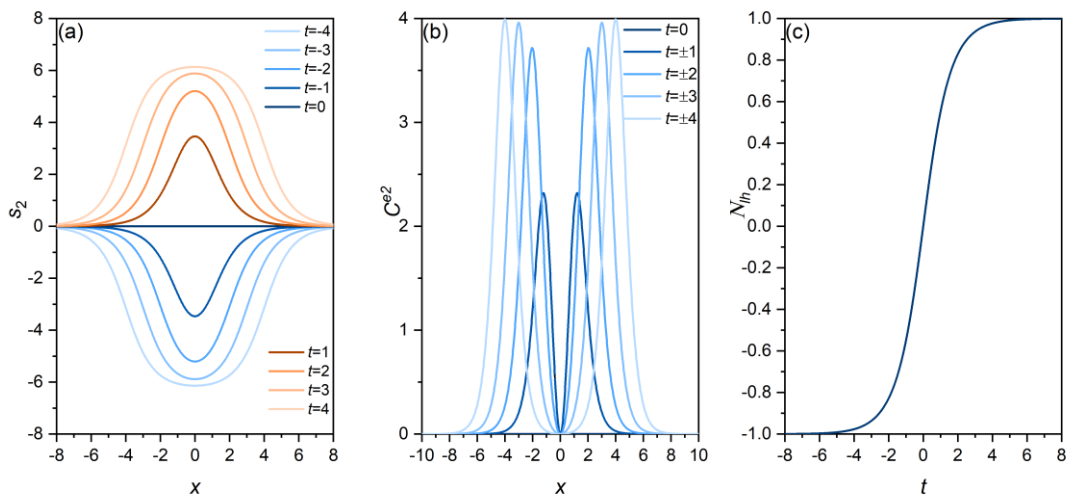


Figure 2. (a) Field pattern and (b) emergent stiffness  $C^{e2}$  of the kink-antikink collision solution of the sine-Gordon model at different values of  $t$ . (c) Variation in the topological charge of the left half-space with  $t$ .

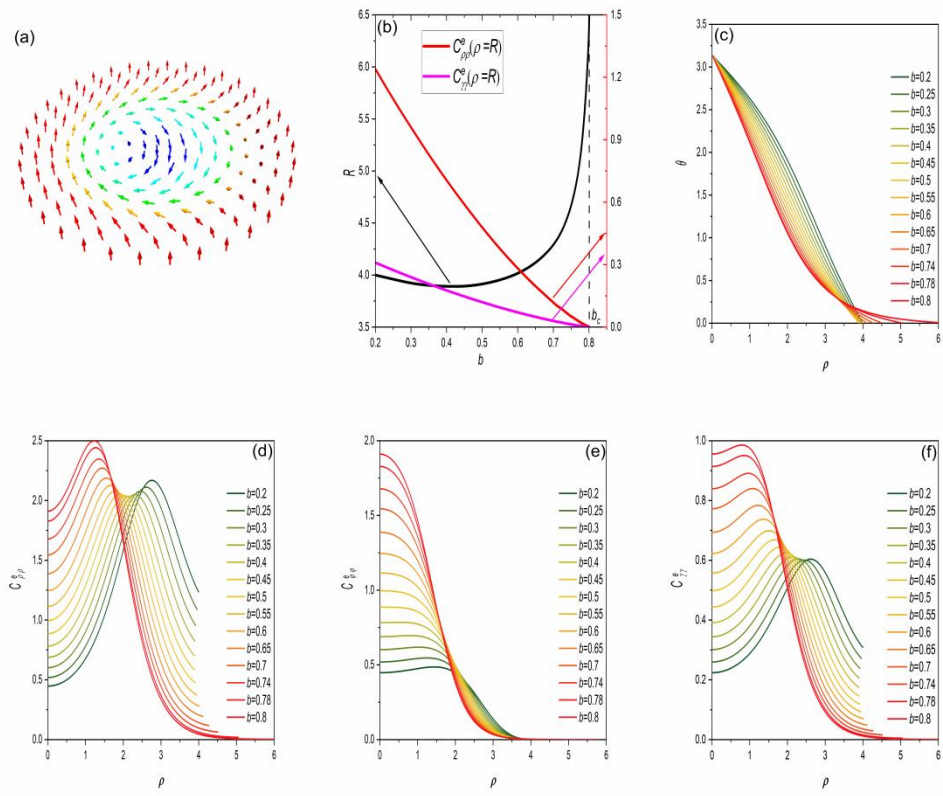


Figure 3. (a) Illustration of the field pattern of a Bloch-type isolated magnetic skyrmion. (b) Variation in  $R$ ,  $C_{\rho\rho}^e(\rho = R)$  and  $C_{\gamma\gamma}^e(\rho = R)$  with  $b$ . Variation in (c)  $\theta$ , (d)  $C_{\rho\rho}^e$ , (e)  $C_{\phi\phi}^e$ , and (f)  $C_{\gamma\gamma}^e$  with  $\rho$  at different values of  $b$ .

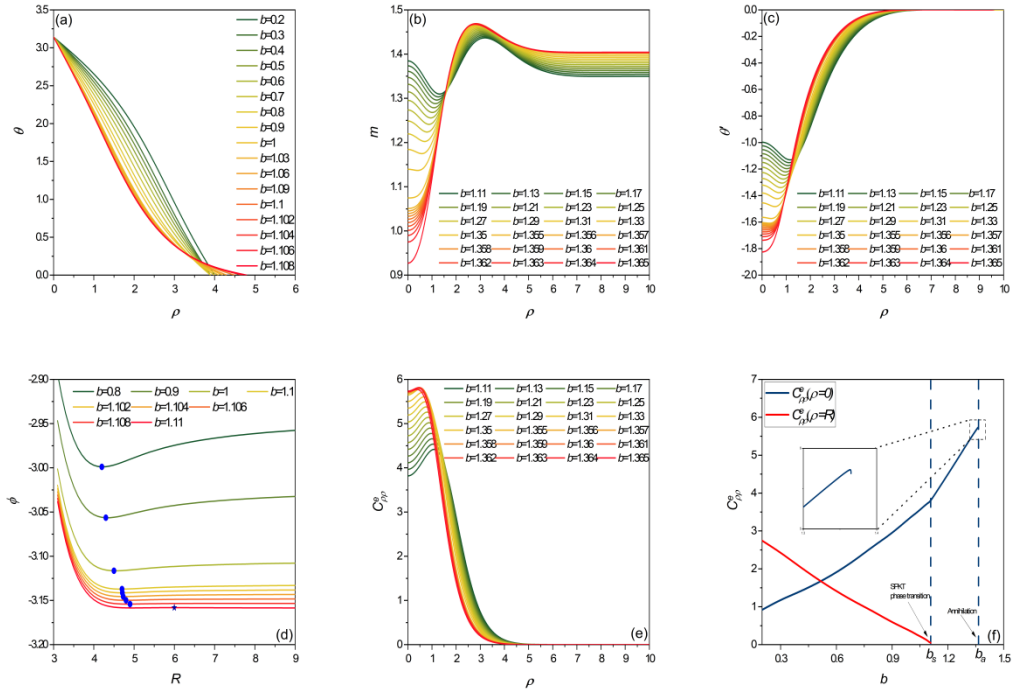


Figure 4. Variation in (a)  $\theta$ , (b)  $m$ , (c)  $\theta'$ , and (e)  $C_{\rho\rho}^e$  with  $\rho$  at different values of  $b$ . (d) Variation in the minimized free energy density  $\phi$  with the radius of an isolated skyrmion  $R$  calculated at different values of  $b$ . The circular blue dots mark the minimum point of the  $\phi - R$  curves calculated at different  $b$ , while the blue star marks the appearance of a local maximum of the  $\phi - R$  curve calculated at  $b = 1.11$ , and  $\phi$  decreases with  $R$  after this point such that the equilibrium  $R$  approaches infinity at  $b = 1.11$ . (f) Variation in  $C_{\rho\rho}^e(\rho = 0)$  and  $C_{\rho\rho}^e(\rho = R)$  with the applied magnetic field  $b$ .